Experimental investigation of the effects of nanosecond repetitive pulsed (NRP) discharges on ignition of methane-air mixtures

A Seydou, Alain Claverie, J. Sotton, M. Bellenoue

Experimental investigation of the effects of nanosecond repetitive pulsed (NRP) discharges on ignition of methane-air mixtures

A. Seydou[1,*], A. Claverie[1], J. Sotton[1], M. Bellenoue[1]
[1]: Institut Pprime, (CNRS, UPR 3346, Université de Poitiers, ENSMA), 1 Av Clément Ader, Téléport 2, BP 40109, 86961 Futuroscope Chasseneuil, France
* Correspondent author: allassane.seydou@ensma.fr

Keywords: NRP discharges, Particle Image Velocimetry, planar laser induced fluorescence, chemiluminescence, ignition, combustion

ABSTRACT

We performed simultaneous planar laser-induced fluorescence (PLIF) and chemiluminescence on OH radical during methane-air mixture ignition and combustion initiated by nanosecond repetitive pulsed (NRP) discharges in a cubic chamber. Single PLIF images are taken at different time delays after the occurrence of the repetitive discharges while chemiluminescence images are synchronized to the discharge and record early stages of the ignition kernel as well as flame propagation. An analysis based on apparent flame velocity of the reactive front is used to understand the ignition process and the observed ignition delay reduction and flame front wrinkling as the number of discharge pulses is increased. In addition, particle image velocimetry (PIV) in an inert airflow was developed in order to characterize the hydrodynamic effects of NRP discharges, namely shock wave and hot kernel relevant to the observed flame properties enhancement. The main objective of this study is to understand the effects of NRP discharges in plasma-flame interactions for a better comprehension of the main physical processes involved in plasma assisted ignition and combustion of hydrocarbon flames.

1. Introduction

One of the most important aspects of thermal engines efficiency enhancement and pollutant reduction lies in the optimization of combustion processes. In this context, low temperature non-equilibrium plasmas have been efficiently used for the last decades to promote ignition and combustion of fuel-containing mixtures. The efficiency is considered in terms of ignition delay reduction [Aleksandrov et al. (1981)], production of active radicals [Yin et al. (2013)], flame stabilization [Pilla G. (2008)] and pollutant formation reduction . Although different phenomena are involved in plasma-assisted ignition/combustion, [Jiguang Ju & Wenting sun (2015)] have identified four different pathways of combustion enhancement by plasma discharges: thermal, chemical, fuel decomposition and hydrodynamic [Bellenoue et al. (2007)] pathways. The influence of each effect is to date not quantified and the complex plasma-flame interaction still remains unresolved. Previous studies [Pilla (2008)], [Tholin et al. (2013)] supported that the mechanisms of

interaction are mainly chemical and thermal effects. Thermal effect consists in a rapid heating of the mixture through translational energy transfert between electrons and molecules, resulting in acceleration of reaction rates as described by the Arrhenius law. Chemical effect corresponds to reactive species and radicals production by highly energetic excited electrons, ions and molecules. This will accelerate chemical reaction rates and can potentially promote the production of new combustion initiation and development pathways. Recently, experimental [Borghese (1988), Xu et al. (2011), Xu (2013)] and numerical studies [Tholin and Bourdon (2013)] have shown interesting results on the hydrodynamic effects of the NRP discharges, namely shock waves in the earlier stages followed by a hot kernel in later stages. These aerodynamic effects potentially play relevant role in plasma-flame interactions [Da Xu (2013)], but their influence is being neglected. Nevertheless, the physico-chemical processes responsible for this optimization remain not well understood. The objective of this experimental work is to highlight the hydrodynamic effects of NRP discharges on ignition of stoechiometric methane-air-N_2 flames for a better comprehension of the main physical processes involted in plasma-flame interaction.

2. Experimental setups and diagnostics

Cubic combustion chamber

The experimental setup for plasma-assisted combustion used in the current study consists in a stainless steel cubic combustion chamber. It is composed of 3 square faces of 66 mm height each and offers a total volume of about 198 mm^3. In order to perform simultaneously OH radical PLIF and chemiluminescence, 2 fused silica windows are mounted on two opposite faces and allow a maximum pressure in the chamber of 4 MPa. The methane-air-N_2 mixture is manually introduced into the combustion chamber through the valve from vacuum to the desired pressure. The pressure inside the combustion chamber was monitored with a Kistler 601 A piezoelectric pressure sensor. The combustion chamber allows single shot experiments and the pressure evolution is only dependent on heat release and thermal loses.

Two cylindrical tungsten electrodes with 1 mm gap distance are mounted onto a micrometric displacement device and placed into the combustion chamber in vertical pin-to-pin configuration, so that the middle of gap is located at the center of the chamber. An adjustment shim is used to control and settle the gap at 1 mm before each experiment to ensure the same experimental conditions. The nanosecond repetitive (NRP) discharges are delivered by a FID GMBF pulse generator (FGP 10-30NM10) of 10 ns duration and maximum voltage amplitude (Umax) and pulse repetition frequency (PRF) of 10 kV and 30 kHz respectively. A high voltage charge resistance Kanthal of R = 50 Ω ±5% is connected to the high voltage part of the electrical

circuit for impedance matching and current signal noise reduction. The discharge voltage and current intensity are measured by means of a high voltage Lecroy PPE20kV probe and pearson coil 6585 sensor respectively, thus the electrical energy of the discharge can then be deduced. Due to different time scales between the NRP discharges and the combustion, the electrical signals (voltage, current) and pressure signal are recorded on a separate oscilloscopes.

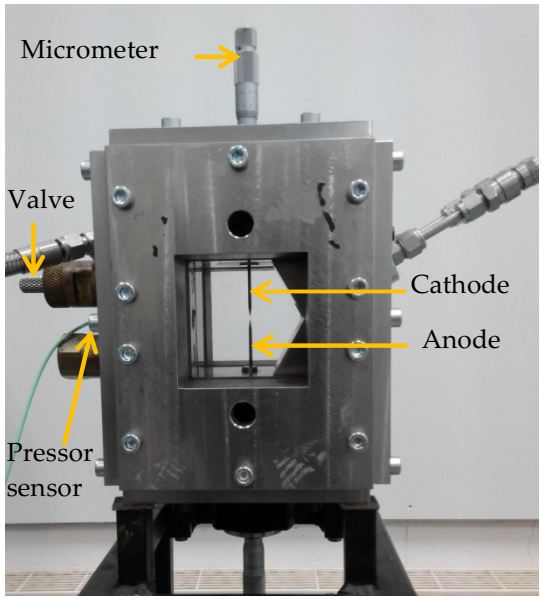

Fig. 1 Cubic constant volume combustion chamber for plasma-assisted combustion

Simultaneous chemiluminescence & PLIF

In the current study, simultaneous chemiluminescence and planar laser-induced fluorescence on the OH radical were performed in order to record the early stages of ignition and the overall combustion development of methane-air mixtures initiated by NRP discharges. For this purpose, we used a Photron SAZ high speed camera of 30 kHz frequency, 1024*1024 pixels resolution and variable exposure time to record chemiluminescence images. This camera is placed perpendicularly to one of the faces of the combustion chamber. A Hamamatsu intensifier with variable amplification gain is connected to the camera in order to improve the low signal to noise ratio. Two extension rings of 16 mm and 8 mm diameter respectively are mounted between the camera and a Bernhard-Halle Nachfl lens with 100 mm focal length, f/2 aperture and bandwidth of [105-405 nm]. This configuration allows us to have near electrode field of 55.3*55.3 mm^2 size within a window of 768*824 $pixels^2$, thus corresponding to a resolution of about 69.5 µm/pixel. Finally, a CVI interference filter centered on 310 nm and 10 nm bandpass is placed in front of the

lens in order to select the OH* radical spontaneous emission during the plasma-assisted ignition/combustion.

In order to perform planar laser-induced fluorescence (PLIF), the OH radical excitation is achieved using a doubled dye laser Continuum ND6000 (with Rhodamine 590) pumped by the second harmonic of a pulsed Nd-YAG Continuum Surelite III laser. The later laser is run at 10 Hz by a Stanford DG645 pulse and delay generator. The tunable dye-laser beam enables to get a wavelength corresponding to the Q_1 (6) absorption band of OH around 282.9 nm with precision on the order of 1 picometer. The laser provides pulses of about 6 ns duration and reaches a maximum energy and frequency of around 15 mJ and 10 Hz respectively. A cylindrical lens was placed at the exit of laser in order to generate a 30 mm height, 500 μm width and 10 mJ energy laser sheet that illuminate a region located at around 1 mm behind the electrode gap position. The energy level and laser characteristics obtained in this study follow the linear regime of OH radical fluorescence (Bresson 2000). An intensified Princeton PI-Max 4 CCD camera with maximum frequency of 5 Hz when using 1024*1024 pixels^2 resolution is placed at the opposite side to record the OH radical 2D fluorescence signal. The coupled intensifier allows nearly 100% amplification gain of the initial signal and acquisition duration as short as 100 ns. This short duration of the amplification avoids collecting OH* chemiluminescence and phosphorescence signals (characteristic time of about 1 ms). A Nikon lens of 105 focal length and f/2.8 maximum aperture is placed on the camera and supports a set of bandpass filters Scott WG280 and UG11 centered around 310 mm to select OH fluorescence wavelength only and avoid background scattering. The acquisition region obtained in this case is a 27*27 mm^2 size square for a resolution of around 26.4 μm/pixel.

Due to different characteristics times of the devices, a precise synchronization scheme was set up in order to perform simultaneous chemiluminescence and PLIF on the OH radical and guaranty the reliability of the results. A single shot PLIF image is coupled to the time-resolved chemiluminescence film. We use the delay generator 1 as master clock of the 10 Hz PLIF laser that delivers a trigger signal to Photron SAZ rapid camera operating at 30 kHz with 25 μs gate time (see figure 2). The output signal of this camera controls and triggers NRP discharges that operate with the same frequency, thus chemiluminescence images are systematically recorded during and after the discharge pulses. A 23 μs gate time intensifier was used to lower the integration time and avoid glare light on the camera sensor especially during the first moments after the pulses. The chemiluminescence images correspond then to the time interval between the pulses. The 100 ns gate time intensified camera (PI-Max 4) is delayed with the desired delay time after the discharges initiation at which a PLIF image is taken. This way, we record single shot image of PLIF at a specific

delay time after the ignition and the entire high speed video of chemiluminescence within the region of interest recording the discharge application as well as resulting flame propagation.

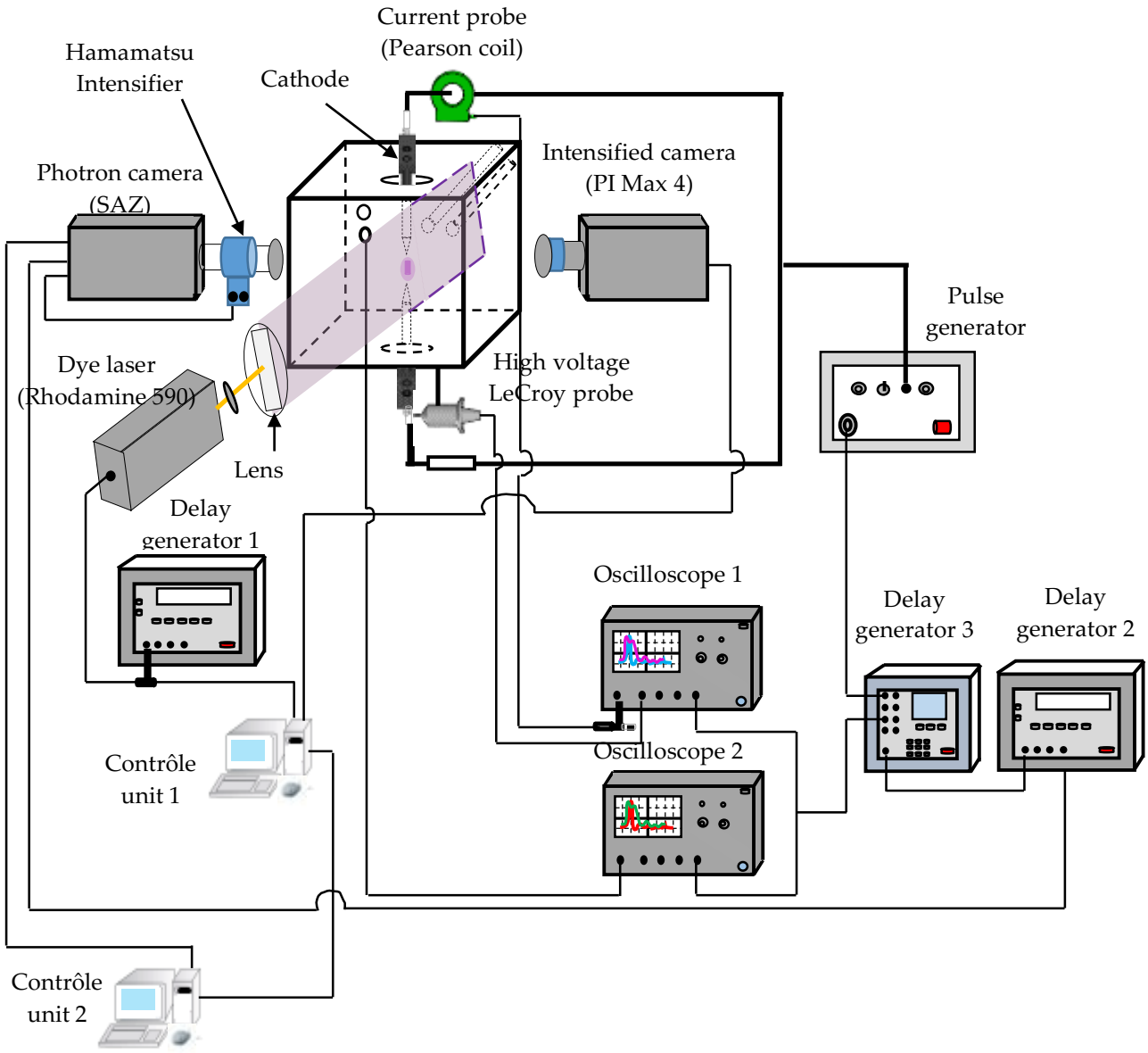

Fig. 2 Experimental setup of simultaneous PLIF and chemiluminescence of OH radical in methane-air-N2 flames.

Particle image velocimetry (PIV):

In order to study plasma-flow interaction, NRP discharges are applied in an atmospheric pressure airflow. This inert flow is seeded with grape seed oil particles with a velocity of around 0.2 m/s. Particle image velocimetry enables to obtain a 2-D velocity field of the 14*11 mm^2 visualization zone centered on the electrodes position. A 10 Hz pulsed Nd-Yag laser (Quantel CFR 200) of 532 nm wavelength is used to illuminate the seeding particles. The thin laser sheet of 200 μm width, 12 ns duration and 100 mJ of maximum energy is directed towards the gap while a CCD Camera (Flow Master 3S CCD) of 1280* 1024 pixels resolution and 8 Hz frequency collects the Mie-scattering of particles in the region of interest, with a maximum resolution of 11 µm/pixel. A couple of frames is recorded before each experiment to determine the flow field before the discharge and a second couple of frames is taken for various delays after the discharge. The minimum time delay between two consecutive laser pulses of our PIV device was $dt_{Laser} = 2$ µs. The precision of velocity measurement was estimated around 0.05 m/s.

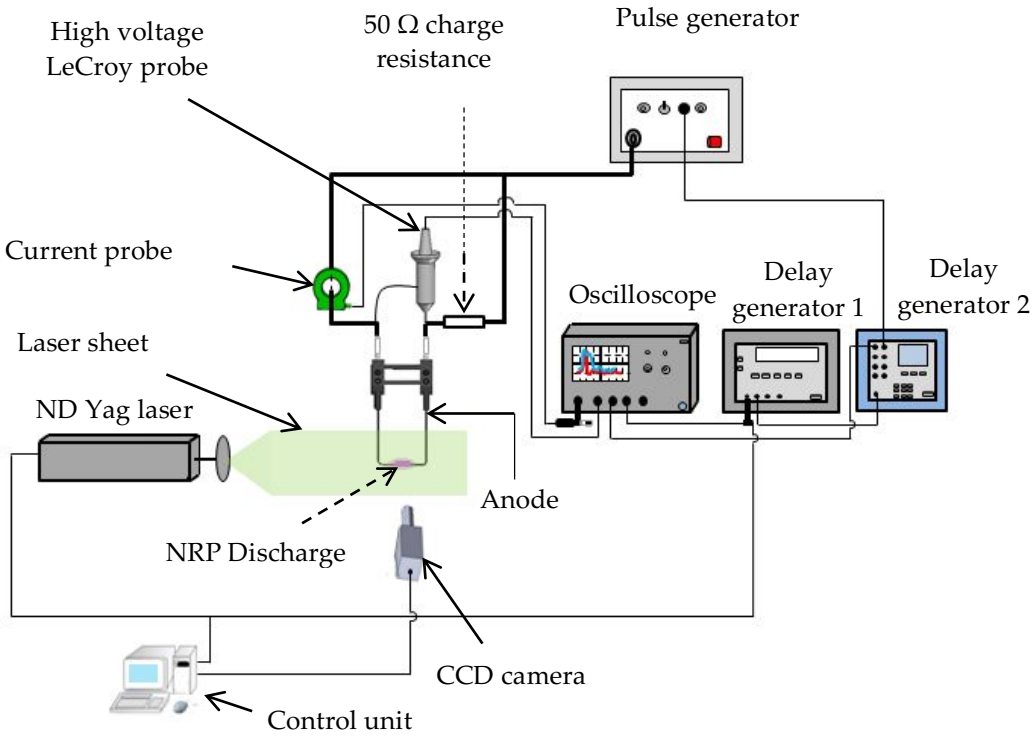

Fig. 3 Experimental setup of particle image velocimetry in quiescent air.

In order to synchronize the different elements of the PIV system, a reference trigger signal from the control unit, is simultaneously sent to the 10 Hz laser and the delay generator (DG) 1. Firstly, the synchronized camera and laser device takes a couple of frames of the "undisturbed" medium. The signal is then delayed by a delay time Δt and sent to the delay generator 2 that launches the discharge pulses. The basic idea is to set a delay time Δt, so that the discharge pulse(s) end(s) at an instant "Dly" before the second couple of frames (located 100 ms after the first one). The value of Dly was varied from 1 µs to 10 µs for the shock wave propagation and from 33 µs to 100 µs for the hot kernel development. The maximum jitter between the delay generator 2 and the discharge was found to be around 500 ns. By this method, hydrodynamic effects of the train of the NRP discharges are highlighted. The resulting chronogram of the synchronization methodology is displayed below.

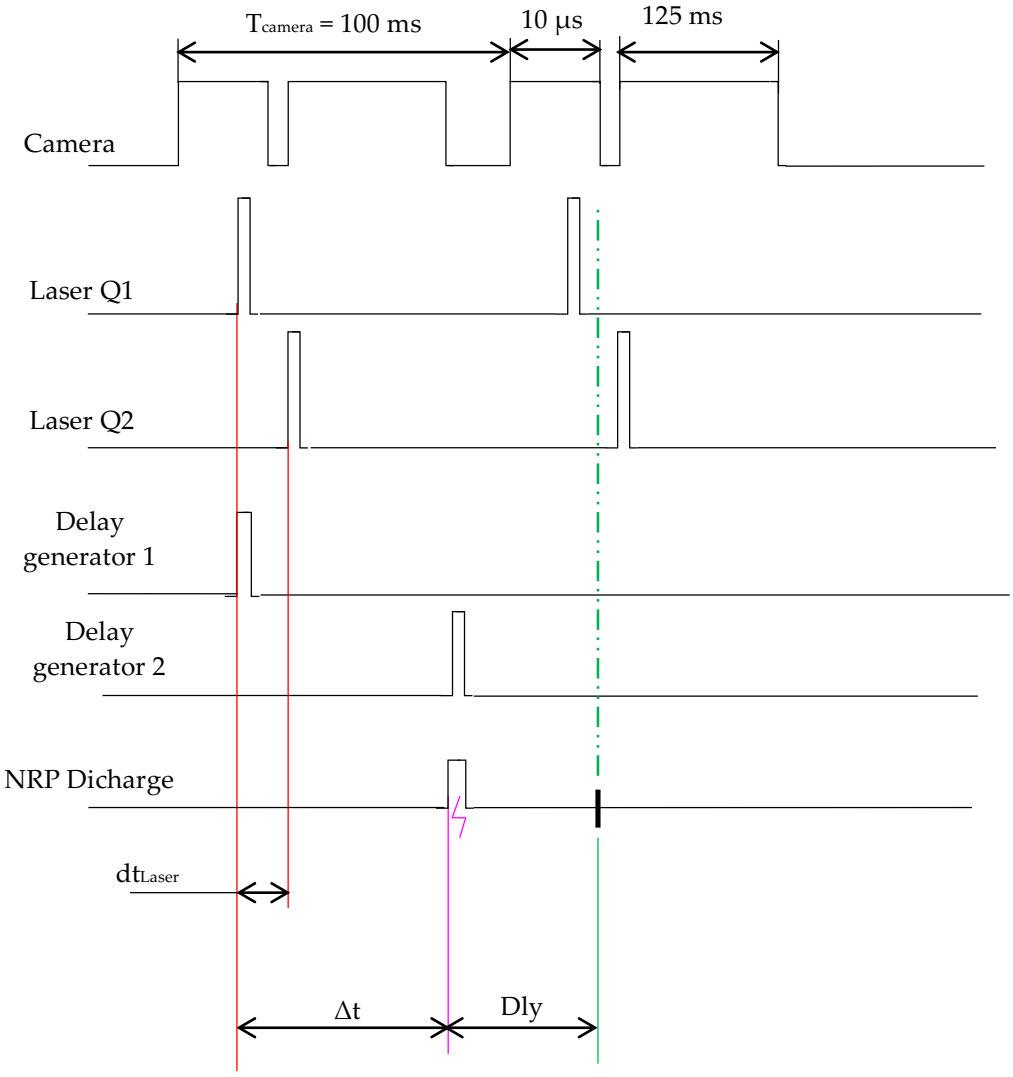

Fig. 4 Chronogram of synchronization methodology for PIV measurements

3. Results and discussion

Stoichiometric quiescent methane-air-N_2 mixture diluted with 20% mass of N_2 is ignited using a burst of 4, 23 and 40 NRP pulses corresponding respectively to 3.9 mJ, 18.31 and 32.07 mJ electrical energy. The initial pressure and temperature are set to P_0 = 1 bar and T_0 = 300 K respectively. The different experiments were carried out in identical conditions. For this mixture, the minimum number of pulses that lead to successful ignition was found to be about 4 pulses. The mean electrical energy was equal to 1.5 mJ for the first pulse and about 0.8 mJ for the subsequent pulses. This can be explained as follows: the first pulse is applied in a fresh medium, so it requires high voltage to overcome the electrical resistance of the gap and produce the spark. The subsequent pulses take place in a medium which could contain intermediate species and residual heat from the previous pulse(s). After the ignition, the flame develops outwardly within the region of interest. For each discharge burst, single shot PLIF images on the OH radical taken respectively at 1ms, 2 ms and 3 ms after the discharge pulses and their corresponding OH* chemiluminescence images are displayed in figure 5. Each couple of images corresponds to a single experiment so that the two simultaneous diagnostics provide complementary information about geometrical aspects of flame front structure. At 1 ms after the ignition, the small flame kernel is not enough developed to reach the acquisition area where the laser sheet is located. This explains why PLIF OH signal intensity is low at 1 ms for 4 pulses. The produced PLIF OH signal then slowly increases until 3 ms. When we increase the number of pulses up to 23 and 40 pulses, the OH signal intensity dramatically increases and the flame already spreads out of the gap in comparison to the same instants as for 4 pulses. Furthermore, the flame front is more distorted as the number of pulses is increased. This is clearly visible on PLIF images. We did not take a PLIF image at 1 ms under 40 pulses simply because at this instant, the discharge pulses are not finished yet. Qualitative chemiluminescence allows 3 dimensional integration of the OH* spontaneous emission along the depth of field. Nevertheless, the wrinkled flame front shape can easily be distinguished as the number of pulses increases and it corresponds approximately to that of PLIF for each experiment.

PLIF

Chimiluminescence

4 Pulses

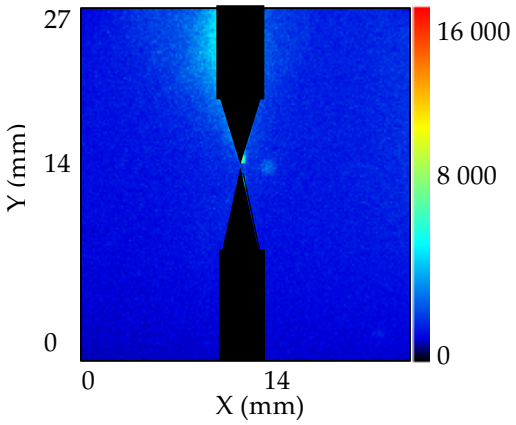

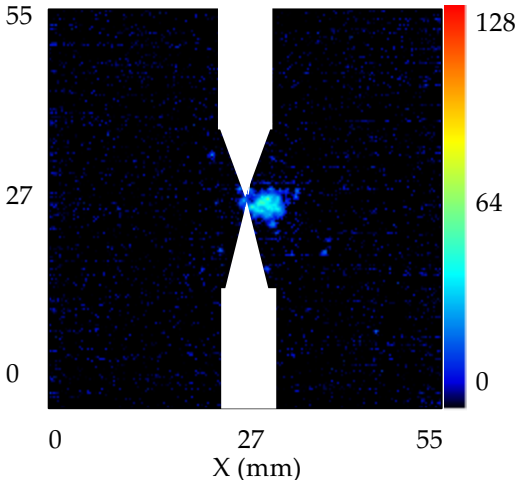

23 Pulses

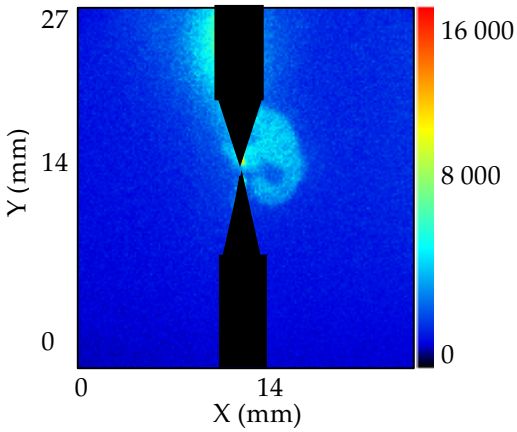

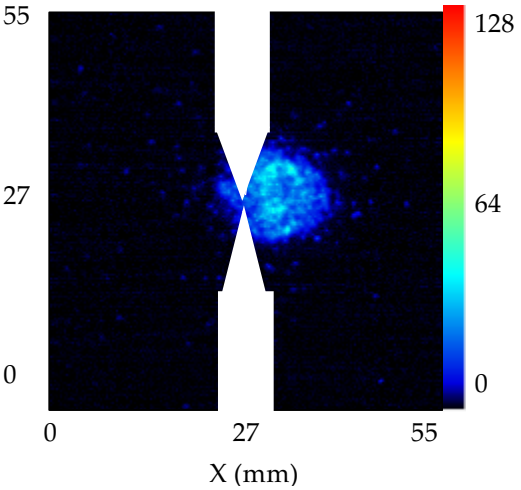

40 Pulses

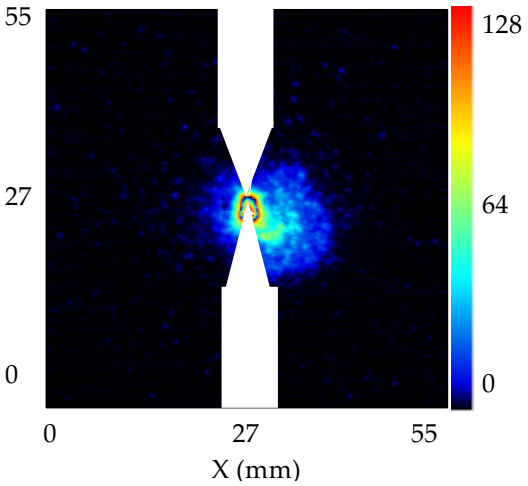

I. Dly=1ms

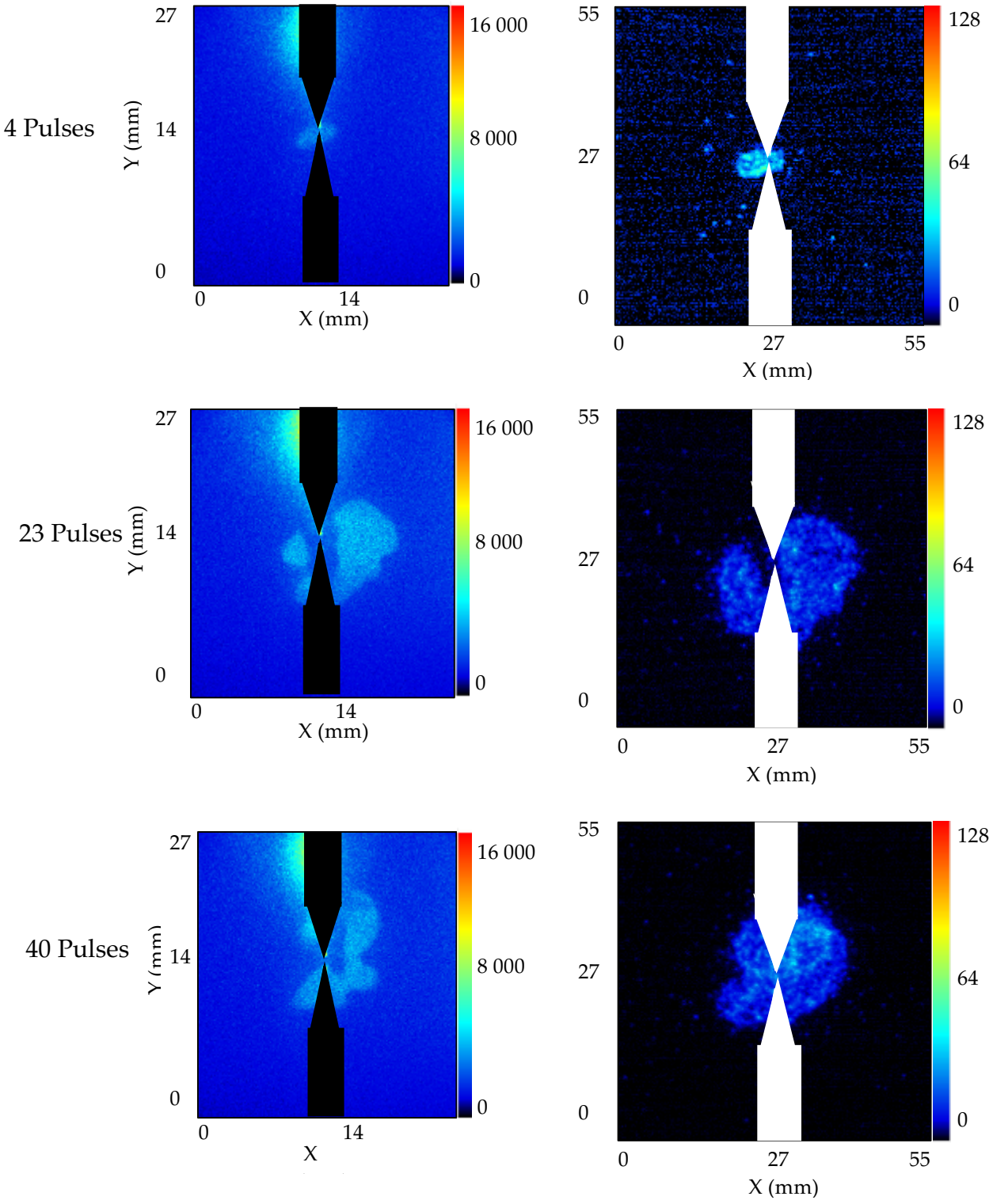
4 Pulses
23 Pulses
40 Pulses
Y (mm)
X (mm)
X
27
14
0
55
16 000
8 000
128
64

II. Dly=2ms

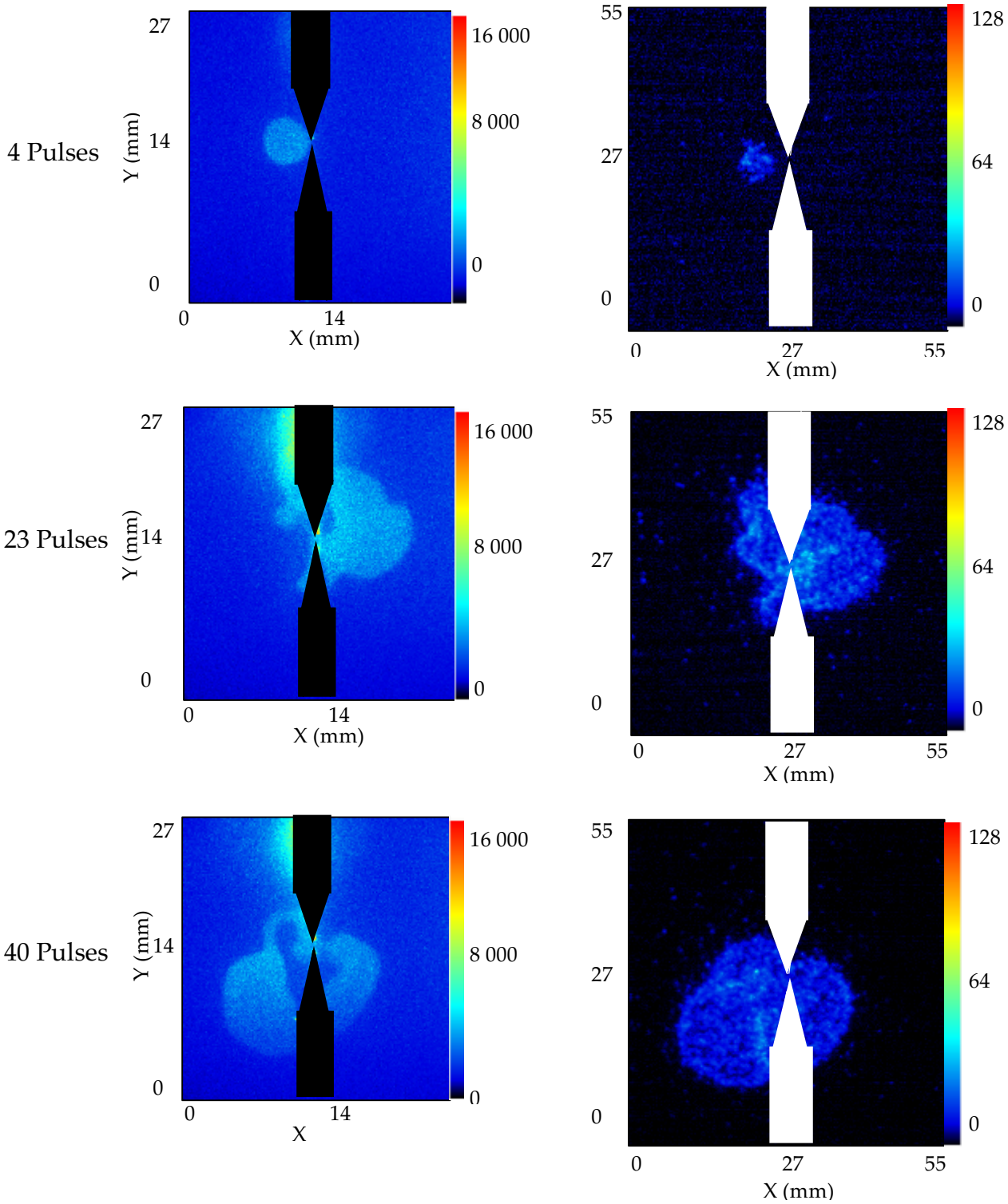

III. Dly=3ms

Fig. 5 Simultaneous OH radical PLIF and OH chemiluminescence images at different instants of methane-air-N_2 mixture ignition by 4, 23 and 40 NRP pulses. P_0 = 1 bar, T_0 = 300 K.

Quantitative analysis:

From chemiluminescence images, we can extract the temporal contour of the flame front within the region of interest as the flame propagates outwardly after ignition. Otsu's algorithm is used for the binarization of chemiluminescence images in order to detect time evolution of flame contour. We define an equivalent flame radius (R_{eq}) based on the surface. The apparent velocity is obtained by calculating the ratio of the average distance between two consecutive flame contours and the corresponding time step. A centered finite differencing scheme with second order accuracy is used to calculate an average of the apparent flame velocity in the frame laboratory's reference:

$$S_a = 2\frac{A_{n+1} + A_{n-1}}{(L_{n+1} + L_{n-1})(t_{n+1} - t_{n-1})}$$

Where A_n is the area inside the contour and L_n is the contour length at the time step tn. Color range goes from red for the earlier stages to blue as the flame propagates.

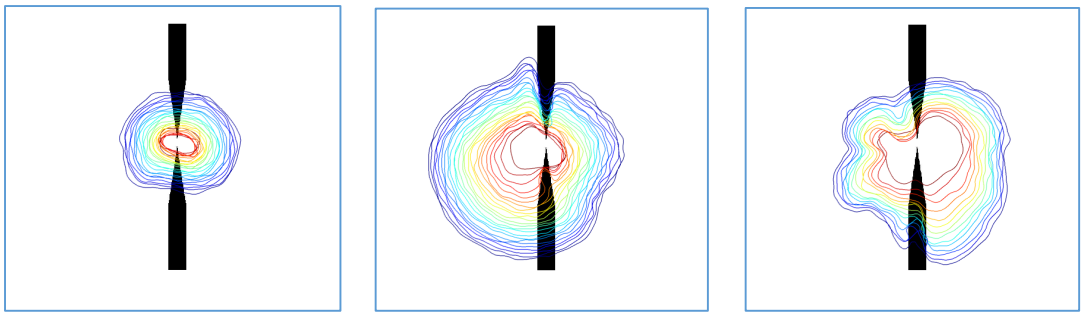

a b c

Fig. 6 Time evolution of flame front contours for a) 4 pulses, b) 23 pulses and c) 40 pulses. Time step = 400 µs

Fig. 6 displays time evolution of flame contour up to 10 ms after the initiation of the discharge under respectively 4, 23 and 40 pulses. It can be noticed that the flame develops outwardly and reaches the region of interest boundaries quite earlier as the number of pulses increases from 4 to 40 pulses. For each case, the first contour obtained 33 µs after the end of pulses is also more developed when the pulse number increases and its size corresponds approximately to that of the hot kernel as it will later be shown in PIV images (see figure 8 below). The contours are also more distorted as seen by simultaneous PLIF and chemiluminescence.

Time evolution of flame equivalent radius is shown in figure 7.a and follows monotonic linear evolution with increasing values from 4 to 40 pulses. Fig. 7.b displays apparent velocity as function of flame radius for 4, 23 and 40 pulses. It can be noticed that for the same equivalent radius the apparent velocity of the flame increases as the number of pulses increases. Before 6 ms, the apparent velocities in case of 23 and 40 pulses are higher than that of 4 pulses, thus confirming the observation of simultaneous PLIF and chemiluminescence images. The apparent flame velocity reaches a steady-state value around 3.7 m/s irrespectively of the number of pulses, suggesting that the enhancement effect occurs at early stages of discharge application and ignition. This can be explained by a more pronounced hydrodynamic effects that enhance mixing and reaction rate as the number of pulses (energy) increases.

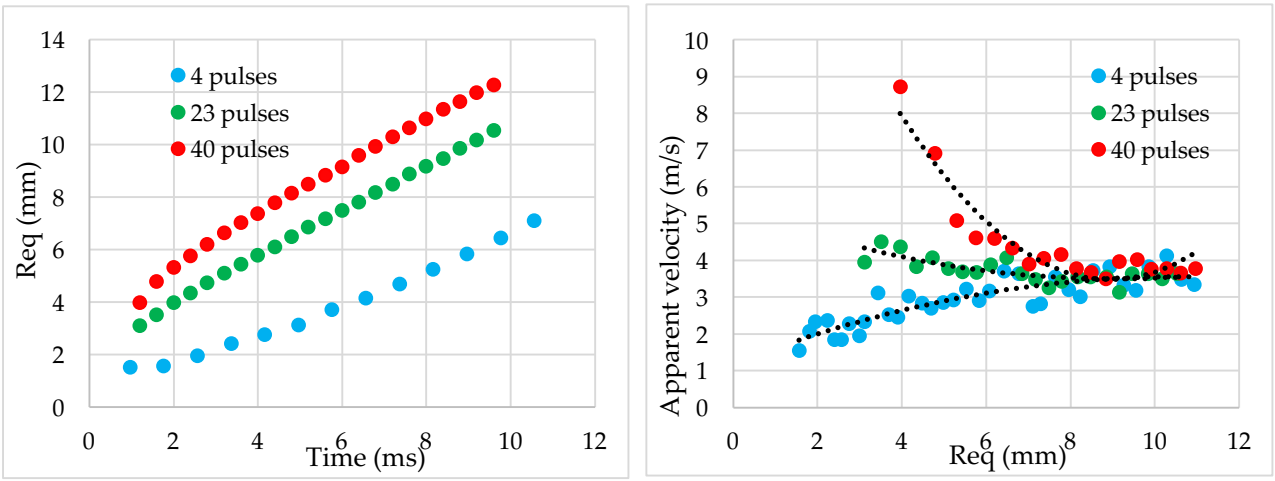

a b

Fig. 7 a) Time evolution of equivalence radius and a) and b) apparent flame velocity function of equivalent radius for atmospheric pressure methane-air-N_2 mixtures ignited with 4, 23 and 40 NRP pulses.

Hydrodynamic effects of NRP discharges

When a discharge is applied in a gas or a combustible mixture, the instantaneous intense energy release produces a spherical shock wave that propagates outwards from the gap center. This phenomenon takes place few microseconds after the discharge and is followed by a hot plasma kernel from residual heat at time scales of tens of microseconds. Initially, the shock wave is cylindrical supersonic and progressively becomes spherical sonic wave due to electrodes configuration as it can be seen in figure 9.a.

The ensuing competition between spherical and cylindrical expansion in the spark gap and the boundary layer on the electrode surface both generate vorticity, resulting in the toroidal shape of the hot gas kernel and enhanced mixing [Bane et al. (2014)]. The repetition of discharge pulses at a high frequency produces subsequent shock waves and increases the hot kernel size, thus amplifying density gradient and momentum transfer around the electrodes (see figure 8). This results in larger instabilities that modify local aerodynamic conditions of the media by heat transfer to electrodes and specific small scale flow prior to ignition. Particle image velocimetry (PIV) images displayed in figure 8 are respectively taken 9 µs and 33 µs after 1 pulse of 1.5 mJ and 10 pulses of 8.7 mJ electrical energy show a spherical shock wave and hot kernel mentioned above.

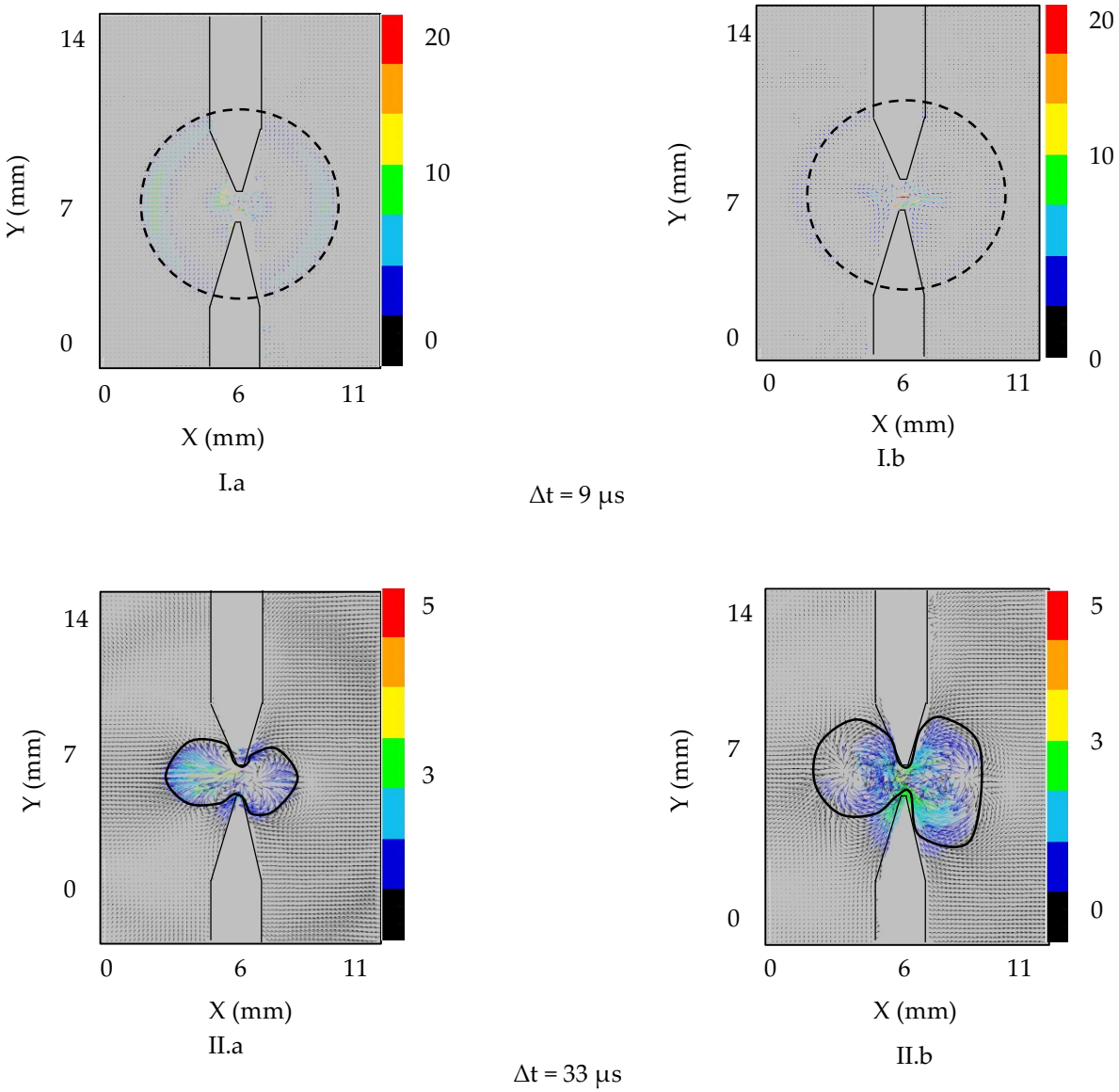

Fig. 8 PIV images of induced shock waves and recirculation by a) 1 pulse (E_{1p}1.5 mJ) and b) 10 pulses (E_{10p}=8.7 mJ) in air at Δt=9 µs and Δt=33 µs. V_{air}=0.2 m/s, P=1 atm, T_{air}=300 K.

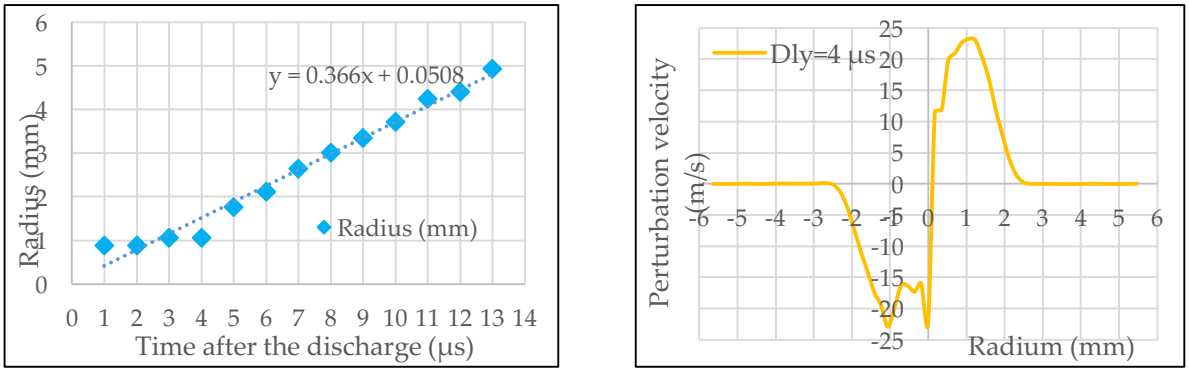

a b

Fig. 9 a) Time evolution and b) radial profile of the maximum amplitude of induced perturbation velocity at Dly=4µs. 1 pulse (E_{ip}=1.5 mJ) in atmospheric pressure air

Besides thermal and chemical effects, ignition and combustion of methane-air mixtures are enhanced due to local aerodynamic effects as the deposited energy (number of pulses) of NRP discharges increases. This observation can be explained as follows: when the deposited energy (number of pulses) increases, a hot plasma kernel and a recirculation zone are formed prior to ignition, that lead to earlier formation of ignition kernel. Initially, the toroidal hot kernel largely influences the ignition. Additional pulses tend to increase the size of the hot kernel and enhance mixing around the electrodes as showed in figure 8. As 4 pulses are sufficient to ignite the mixture, the hot kernel obtained from the repetition of pulses influences the ignition to a certain extent, typically the hot kernel area. When the flame develops sufficiently away from this area, spherical shock waves that pass through the flame front are dominant on propagation and acceleration as we observed by simultaneous chemiluminescence and PLIF. Indeed, the ignition kernel is an interface of strong density gradients while successive spherical shock waves generate pressure gradients (see figure 9.b) along the interface. The simultaneous presence of misaligned density and pressure gradients at the interface produces vorticity that enhances mixing and disturbs the flame front. Because of these baroclinic effects, the flame front is more and more wrinkled and additional instabilities are generated. Thus, local reaction rate increases [Oran and Gardner (1985)] and favors ignition and flame velocity increase. Similar results on flame speed enhancement of lean propane air flames under NRP discharges were obtained by [Xu D. (2013)].

4. Conclusion

The current study gives insight on aerodynamic effects of NRP discharges on methane-air mixtures ignition as well as significant information about morphological aspects of flames. These effects modify local aerodynamic conditions prior, during and after ignition and combustion. PIV results are used to describe aerodynamic effects of NRP discharges and interpret flame kernel development observed by simultaneous OH chemiluminescence and PLIF imaging. Thus, aerodynamic effects of NRP must be considered along with thermal and chemical effects for validating numerical codes for future design of reliable, energy-efficient, low cost and environmentally friendly automotive and aerospace engines. These original and interesting results contribute to a better understanding of the main physical processes involved in plasma assisted ignition and combustion.

Acknowledgements:
This work is supported by ANR-PLASMAFLAME-2011BS0902501 project.

5. References

Aleksandrov N. L., Vysikailo F. I., Islamov R. S., Kochetov I. V., Napartovich A. P., and Pevgov V. G. Electron Distribution Function in 4:1 N_2-O_2 Mixture. [Journal]. - Teplofizika Vysokikh Temperatur, vol. 19, Jan.-Feb. 1981, p. 22-27.High Temperature Science, vol. 19, no. 1, July 1981, p. 17-21

Bane et al. Investigation of the Effect of Electrode Geometry on Spark Ignition. Combustion and Flame 162 (2015) 462–469

Bellenoue M., Labuda S., Ruttun B. and Sotton J. Spark Plug and Corona Abilities to ignite Stoichionetric and Lean Methane-Air Mixtures", Combustion Science and Technology, vol 179, 2007, pp 477-496

Borghese A., D'Alessio A., Diana M. and Venitozzi C. Development of Nitrogen Kernel Produced by a Very Fast Spark Discharge. [Journal]. - Twenty-Second Symposium (International) on Combustion/ The Combustion Institute, 1988/pp. 1651-1569

Bresson A. Techniques d'Imagerie Quantitatives: Fluorescence Induite par Laser Appliquées aux Ecoulements et aux Combustion. PhD Thesis, Université de Rouen, (2000)

Ju Y. and Sun W. Plasma Assisted Combustion: Dynamics and Chemistry. Progress in Energy and Combustion Science 48 (2015) 21-83

Oran E. S., Grandner J. H. Chemical-Acoustic Interactions in Combustion Systems. [Journal]. - Prog. Energy Combust. Sci. 1985, Vol 11-pp. 253 276

Pilla G. Etude Expérimentale de la Stabilisation de Flammes Propane-Air de Prémélange par Décharges Nanosecondes Impulsionnelles Répétitives. PhD Thesis, Ecole Centrale Paris - Laboratoire EM2C, (2008)

Tholin F. et al. Influence of Fast-Heating Processes and O Atom Production by a Nanosecond Spark Discharge on the Ignition of a Lean H_2–Air Premixed Flame. Combust. Flame (2013), http://dx.doi.org/10.1016/j.combustflame.2013.11.007

Tholin F. and Bourdon A. Simulation of the Hydrodynamic Expansion Following a Nanosecond Pulsed Spark Discharge in Air at Atmospheric Pressure. J. Phys. D: Appl. Phys.46 (2013) 365205 (18pp)

Xu Da A., Lacoste Deanna A., Rusterholtz Diane L., Elias Paul-Quentin, Stancu Gabi D. et al. Experimental Study of the Hydrodynamic Expansion following a Nanosecond Repetitively Pulsed Discharge in Air. APPLIED PHYSICS LETTERS 99, 121502 (2011)

Xu D. Thermal and Hydrodynamic Effects of Nanosecond Discharges in Air and Application to Plasma-Assisted Combustion. PhD Thesis, Ecole Centrale Paris - Laboratoire EM2C, (2013)

Yin et al. OH Radical and Temperature Measurements during Ignition of H_2-Air Mixtures Excited by a Repetitively Pulsed Nanosecond Discharge. Proceedings of the Combustion Institute 34 (2013) 3249–3258